

1 **Concentration, sources and light absorption**  
2 **characteristics of dissolved organic carbon on a medium**  
3 **sized valley glacier, northern Tibetan Plateau**

4 **F. Yan<sup>1,4,5</sup>, S. Kang<sup>1,3</sup>, C. Li<sup>2,3</sup>, Y. Zhang<sup>1</sup>, X. Qin<sup>1</sup>, Y. Li<sup>2,4</sup>, X. Zhang<sup>1,4</sup>, Z. Hu<sup>1,4</sup>, P. Chen<sup>2</sup>, X. Li<sup>1</sup>, B.**  
5 **Qu<sup>5</sup>, M. Sillanpää<sup>5,6</sup>**

6 <sup>1</sup>Qilian Station for Glaciology and Ecological Environment, State Key Laboratory of Cryospheric  
7 Sciences, Northwest Institute of Eco-Environment and Resources, Chinese Academy of Sciences,  
8 Lanzhou 730000, China

9 <sup>2</sup>Key Laboratory of Tibetan Environment Changes and Land Surface Processes, Institute of Tibetan  
10 Plateau Research, Chinese Academy of Sciences, Beijing 100101, China

11 <sup>3</sup>CAS Center for Excellence in Tibetan Plateau Earth Sciences, Chinese Academy of Sciences, Beijing  
12 100101, China

13 <sup>4</sup>University of Chinese Academy of Sciences, Beijing 100049, China

14 <sup>5</sup>Laboratory of Green Chemistry, Lappeenranta University of Technology, Mikkeli, Sammonkatu 12,  
15 FIN-50130, Finland

16 <sup>6</sup>Department of Civil and Environmental Engineering, Florida International University, Miami, FL  
17 33174, USA

18 Correspondence to: S. Kang (shichang.kang@lzb.ac.cn), C. Li (lichao.li@itpcas.ac.cn)

19 **Abstract.** Light-absorbing dissolved organic carbon (DOC) constitutes a major part of the organic  
20 carbon in glacierized regions, and has important influences on the carbon cycle and radiative forcing of  
21 glaciers. However, few DOC data are currently available from the glacierized regions of the Tibetan  
22 Plateau (TP). In this study, DOC characteristics of a medium sized valley glacier (Laohugou Glacier  
23 No. 12 (LHG Glacier)) on the northern TP were investigated. Generally, DOC concentrations on LHG  
24 Glacier were comparable to those in other regions around the world. DOC concentrations in snowpits,  
25 surface snow and surface ice (superimposed ice) were  $332 \pm 132 \mu\text{g L}^{-1}$ ,  $229 \pm 104 \mu\text{g L}^{-1}$  and  $426 \pm$   
26  $270 \mu\text{g L}^{-1}$ , respectively. The average discharge-weighted DOC of proglacial streamwater was  $238 \pm 96$   
27  $\mu\text{g L}^{-1}$ , and the annual DOC flux released from this glacier was estimated to be  $6,949 \text{ kg C yr}^{-1}$ , of  
28 which 46.2 % of DOC was bioavailable and could be decomposed into  $\text{CO}_2$  within one month of its

29 release. The mass absorption cross section (MAC) of DOC at 365 nm was  $1.4 \pm 0.4 \text{ m}^2 \text{ g}^{-1}$  in snow and  
30  $1.3 \pm 0.7 \text{ m}^2 \text{ g}^{-1}$  in ice, similar to the values for dust transported from adjacent deserts. Moreover, there  
31 was a significant relationship between DOC and  $\text{Ca}^{2+}$ , therefore, mineral dust transported from adjacent  
32 arid regions likely made important contributions to DOC of the glacierized regions, although  
33 contributions from autochthonous carbon and autochthonous/heterotrophic microbial activity cannot be  
34 ruled out. The radiative forcing of snowpit DOC was calculated to be  $0.43 \text{ W m}^{-2}$ , demonstrating that  
35 DOC in snow need to be taken into consideration in accelerating melt of glaciers on the TP.

36 **Key words:** dissolved organic carbon, light absorption, LHG Glacier, the Tibetan Plateau

## 37 **1 Introduction**

38 Ice sheets and mountain glaciers cover 11 % of the land surface of the Earth and store  
39 approximately 6 Pg (1 Pg =  $10^{15}$  g) of organic carbon, the majority of which (77 %) is in the form of  
40 dissolved organic carbon (DOC) (Hood et al., 2015). The annual global DOC release through glacial  
41 runoff is around  $1.04 \pm 0.18$  Tg C (1 Tg =  $10^{12}$  g) (Hood et al., 2015). Therefore, glaciers not only play  
42 an important role in the hydrological cycle by contributing to sea level (Jacob et al., 2012) and  
43 endorheric basins (Neckel et al., 2014), but also potentially influence the global carbon cycle (Anesio  
44 and Laybourn-Parry, 2012; Hood et al., 2015) in the context of accelerated glacial ice loss rates. In  
45 addition, a large portion of glacier-derived DOC has proven to be highly bioavailable, influencing the  
46 balance of downstream ecosystems (Hood et al., 2009; Singer et al., 2012; Spencer et al., 2014).

47 Although DOC storage in ice sheets is much larger than that of mountain glaciers, the annual  
48 mountain glacier-derived DOC dominates the global DOC release (Hood et al., 2015). Currently, there  
49 are studies on DOC concentrations, ages and compositions of glaciers in Alaska (Stubbins et al., 2012;  
50 Hood et al., 2009), DOC bioavailability of glaciers on the Tibetan Plateau and Greenland Ice Sheet  
51 (Spencer et al., 2014; Lawson et al., 2014) and DOC storage and export of the whole glacier regions  
52 around the world (Hood et al., 2015). The sources of glacier DOC are diverse and include  
53 autochthonous or *in situ* biological activities (Anesio et al., 2009), allochthonous carbon derived from  
54 overridden soils and vegetation (Bhatia et al., 2010); terrestrial inputs (DOC deposition from vascular  
55 plants and dust) (Singer et al., 2012) and anthropogenic sources (Stubbins et al., 2012). Research on  
56 glacier microbial activity suggests that globally cryoconite holes alone can potentially fix about 64 Gg  
57 C per year (Anesio et al., 2009). Meanwhile, there are large variations in glacier DOC concentrations  
58 and ages (Singer et al., 2012; Hood et al., 2015; Antony et al., 2011). For example, the concentration of  
59 total organic carbon in snow across the East Antarctic Ice Sheets exhibited remarkable spatial  
60 variations due to the marine source of organic carbon (Antony et al., 2011). Studies of both radiocarbon  
61 isotopic compositions and biodegradable DOC (BDOC) have proposed that ancient organic carbon  
62 from glaciers is much easier for microbes to utilize in glacier-fed rivers and oceans, implying that large  
63 amounts of this DOC will return to the atmosphere quickly as CO<sub>2</sub> and participate in the global carbon  
64 cycle, thereby producing a positive feedback in the global warming process (Hood et al., 2009; Singer  
65 et al., 2012; Spencer et al., 2014).

66 In addition to black carbon (BC), another DOC fraction known as water-soluble brown carbon has

67 also been considered as a warming component in the climate system (Andreae and Gelencsér, 2006;  
68 Chen and Bond, 2010). This type of DOC exhibits strong light-absorbing properties in the ultraviolet  
69 wavelengths (Andreae and Gelencsér, 2006; Chen and Bond, 2010; Cheng et al., 2011). The radiative  
70 forcing caused by water-soluble organic carbon (the same as DOC) relative to BC in aerosols was  
71 estimated to account for 2-10 % in a typical pollution area of North China (Kirillova et al., 2014a) and  
72 approximately 1 % at a remote island in the Indian Ocean (Bosch et al., 2014), respectively.  
73 Unfortunately, to date, few direct evaluations have been conducted in the glacierized regions around the  
74 world, including the Tibetan Plateau (TP), where DOC accounts for a large part of the carbonaceous  
75 matter (Legrand et al., 2013; May et al., 2013) and potentially contributes significantly to the radiative  
76 forcing.

77 The TP has the largest number of glaciers at moderate elevations. Most of the glaciers on the TP  
78 are experiencing intensive retreat because of multiple reasons such as climatic conditions (Kehrwald et  
79 al., 2008; Bolch et al., 2012; Yao et al., 2012; Kang et al., 2015) and anthropogenic carbonaceous  
80 particle deposition (Xu et al., 2009; Lau et al., 2010; Nair et al., 2013; Kaspari et al., 2014). However,  
81 to date, no study has quantitatively evaluated the light absorption characteristics of DOC in the  
82 glacierized regions on the TP, despite some investigations of concentrations, bioavailability and sources  
83 of DOC (Spencer et al., 2014; Yan et al., 2015). The primary results of these studies have shown that  
84 DOC concentrations in snowpits at sites on the northern TP are higher than those on the southern TP  
85 (Yan et al., 2015). In addition, a large fraction of the ancient DOC in the glaciers on the southern TP is  
86 highly bioavailable (Spencer et al., 2014). However, knowledge of DOC in TP glaciers remains lacking  
87 due to the large area and diverse environments of the TP in contrast to the relatively limited samples  
88 and studies. Therefore, this study is to comprehensively investigate the sources, light absorption  
89 properties and carbon dynamics in this glacierized region. The results provide a basis for the study of  
90 DOC across the TP and other regions in the future.

## 91 **2 Methodology**

### 92 **2.1 Study area and sampling site**

93 Laohugou Glacier No. 12 (LHG Glacier) (39°05'-40'N, 96°07'-97°04'E 4260-5481 m) is the largest  
94 mountain glacier (9.85 km, 20.4 km<sup>2</sup>) in the Qilian Mountains and is located on the northeastern edge  
95 of the TP (Du et al., 2008; Dong et al., 2014a). It divides western and eastern branches at the elevation  
96 of 4560 m a.s.l (Dong et al., 2014a). The glacier is surrounded by extensive large arid and semi-arid

97 regions (sandy deserts and the Gobi Desert) and is frequently influenced by strong dust storms (Dong  
98 et al., 2014b) (Fig. 1) and covers an area of approximately 53.6 % of the entire LHG glacier basin (Du  
99 et al., 2008; Li et al., 2012).

100 LHG Glacier has typical continental and arid climate characteristics (Li et al., 2012; Zhang et al.,  
101 2012b). Precipitation from May to September accounts for over 70 % of the annual total amount  
102 (Zhang et al., 2012b). The monthly mean air temperature in the ablation zone of the glacier ranges from  
103 -18.4°C in December to 3.4°C in July (Li et al., 2012). Like other glaciers on the TP, LHG Glacier has  
104 been experiencing significant thinning and shrinkage at an accelerated rate since the mid-1990s (Du et  
105 al., 2008; Zhang et al., 2012b).

## 106 **2.2 Sample collection**

107 Two snowpits were dug in 2014 and 2015 at almost the same location in the accumulation zone of  
108 LHG Glacier. In total, 15 and 23 snow samples were collected from these pits in 2014 and 2015,  
109 respectively, at a vertical resolution of 5 cm. Moreover, 29 surface snow and 42 surface ice samples  
110 were collected along the eastern tributary from the terminus to the accumulation zone at an  
111 approximate elevation interval of 50 or 100 m, and 201 proglacial streamwater samples were collected  
112 at the gauge station during the melting period (Fig. 1, Table 1). The concentrations of glacier DOC  
113 have been observed to be very low and are prone to contamination, often causing an overestimation of  
114 DOC concentrations (Legrand et al., 2013). Therefore, before sample collection, polycarbonate bottles  
115 were firstly washed three times by ultrapure water, then soaked with 1 M HCl for 24 h (Spencer et al.,  
116 2009), rinsed three times using ultrapure water, then finally soaked in ultrapure water for over 24 h.  
117 Throughout the sampling period, snow samples were collected directly into 125-mL pre-cleaned bottles,  
118 surface ice (0-3 cm and 3-5 cm) samples were collected using an ice axe directly into polycarbonate  
119 bottles after crushing, while proglacial streamwater samples were filtered immediately after collection  
120 before being transferred into bottles. All ice and snow sample were filtered as soon as possible after  
121 they were melted. To prevent contamination, sampling personnel were careful to avoid touching any  
122 other surfaces whilst carrying out the sample collection. At least one blank was made for every  
123 sampling process to confirm that the contamination was low (Table S1). Meanwhile, another batch of  
124 samples was also collected for BC analysis following the protocol discussed in detail in our earlier  
125 study (Qu et al., 2014); these results are subjected to future work. In order to evaluate DOC discharge  
126 from the entire TP, DOC concentrations in proglacial streamwater samples from a further five glaciers

127 were also measured during monsoon and non-monsoon seasons (Fig. 1, Table S2).

128 All the collected samples were kept frozen and in the dark during storage in the field,  
129 transportation and in the laboratory until analysis. In addition, four dust fall samples from Dunhuang, a  
130 desert location (39°53'-41°35'N, 92°13'-93°30'E) and potential source region for dust deposited on LHG  
131 Glacier, were collected to compare the light absorption characteristics of dust-sourced DOC to those of  
132 the snowpit and ice samples. Mineral and elemental compositions of desert sands of west China have  
133 been homogenized by aeolian activity (Hattori et al., 2003), so that the dust samples collected in this  
134 study are representative of desert sourced dust in west China.

## 135 **2.3 Laboratory analyses**

### 136 **2.3.1 Concentration measurements of DOC and major ions**

137 DOC concentrations were determined using a TOC-5000A analyzer (Shimadzu Corp, Kyoto,  
138 Japan) following filtration through a PTFE membrane filter with 0.45- $\mu\text{m}$  pore size (Macherey–Nagel)  
139 (Yan et al., 2015). The detection limit of the analyzer was 15  $\mu\text{g L}^{-1}$ , and the average DOC  
140 concentration of the blanks was  $32 \pm 7 \mu\text{g L}^{-1}$ , demonstrating that contamination can be ignored during  
141 the pre-treatment and analysis processing of these samples (Table S1). The major cations ( $\text{Ca}^{2+}$ ,  $\text{Mg}^{2+}$ ,  
142  $\text{Na}^+$ ,  $\text{K}^+$  and  $\text{NH}_4^+$ ) and major anions ( $\text{Cl}^-$ ,  $\text{NO}_3^-$  and  $\text{SO}_4^{2-}$ ) were measured using a Dionex-6000 Ion  
143 Chromatograph and a Dionex-3000 Ion Chromatograph (Dionex, USA), respectively. The detection  
144 limit was 1  $\mu\text{g L}^{-1}$ , and the standard deviation was less than 5 % (Li et al., 2007; Li et al., 2010). The  
145 average ion concentrations of the blanks were very low and could be ignored ( $\text{Na}^+$ ,  $\text{K}^+$ ,  $\text{Mg}^{2+}$ ,  $\text{F}^-$ ,  $\text{SO}_4^{2-}$ ,  
146  $\text{Cl}^-$ ,  $\text{NO}_3^- < 1 \mu\text{g L}^{-1}$ ;  $\text{NH}_4^+ = 1.4 \mu\text{g L}^{-1}$ ;  $\text{Ca}^{2+} = 1.2 \mu\text{g L}^{-1}$ ).

### 147 **2.3.2 Light absorption measurements**

148 The light absorption spectra of DOC samples were measured using an ultraviolet-visible  
149 absorption spectrophotometer (SpectraMax M5, USA), scanning wavelengths from 200-800 nm at a  
150 precision of 5 nm. The mass absorption cross section (MAC) was calculated based on the  
151 Lambert-Beer Law (Bosch et al., 2014; Kirillova et al., 2014a; Kirillova et al., 2014b):

$$152 \quad \text{MAC}_{\text{DOC}} = \frac{-\ln\left(\frac{I}{I_0}\right)}{C \cdot L} = \frac{A}{C \cdot L} \times \ln(10) \quad (1)$$

153 where  $I_0$  and  $I$  are the light intensities of the transmitted light and incident light, respectively;  $A$  is the

154 absorbance derived directly from the spectrophotometer; C is the concentration of DOC; and L is the  
 155 absorbing path length (1 cm).

156 In order to investigate the wavelength dependence of DOC light absorption characteristics, the  
 157 Absorption Ångström Exponent (AAE) was fitted by the following equation (Kirillova et al., 2014a;  
 158 Kirillova et al., 2014b):

$$159 \quad \frac{A(\lambda_1)}{A(\lambda_2)} = \left(\frac{\lambda_2}{\lambda_1}\right)^{AAE} \quad (2)$$

160 AAE values were fitted for wavelengths of 330 to 400 nm; within this wavelength range, light  
 161 absorption by other inorganic compounds (such as nitrate) can be avoided (Cheng et al., 2011). The  
 162 radiative forcing caused by BC has been widely studied (Kaspari et al., 2014; Qu et al., 2014; Ming et  
 163 al., 2013). Therefore, using a simplistic model (the following algorithm) in this study, the amount of  
 164 solar radiation absorbed by DOC compared to BC was estimated:

$$165 \quad f = \frac{\int_{300}^{2500} I_0(\lambda) \cdot \left\{ 1 - e^{-\left(\text{MAC}_{365} \left(\frac{365}{\lambda}\right)^{AAE_{\text{DOC}}}\right) \cdot C_{\text{DOC}} \cdot h_{\text{ABL}}} \right\} d\lambda}{\int_{300}^{2500} I_0(\lambda) \cdot \left\{ 1 - e^{-\left(\text{MAC}_{550} \left(\frac{550}{\lambda}\right)^{AAE_{\text{BC}}}\right) \cdot C_{\text{EC}} \cdot h_{\text{ABL}}} \right\} d\lambda} \quad (3)$$

166 where  $\lambda$  is the wavelength;  $I_0(\lambda)$  is the clear sky solar emission spectrum determined using the Air  
 167 Mass 1 Global Horizontal (AM1GH) irradiance model (Levinson et al., 2010);  $\text{MAC}_{365}$  and  $\text{MAC}_{550}$  are  
 168 the mass absorption cross section of DOC at 365 nm and mass absorption cross section of BC at 550  
 169 nm, respectively;  $h_{\text{ABL}}$  is the vertical height of the atmospheric boundary layer; and  $AAE_{\text{DOC}}$  and  
 170  $AAE_{\text{BC}}$  are the Absorption Ångström Exponents (AAEs) of DOC and BC. In this simplistic model, we  
 171 used  $\text{MAC}_{550} = 7.5 \pm 1.2 \text{ m}^2 \text{ g}^{-1}$  (following Bond and Bergstrom, 2006), AAE for BC was set as 1, and  
 172  $h_{\text{ABL}}$  was set to 1000 m, which has little influence on the integration from the wavelengths of 300-2500  
 173 nm (Bosch et al., 2014; Kirillova et al., 2014a; Kirillova et al., 2014b). It is obvious that the value of f  
 174 is closely connected to the relative concentrations of DOC and BC.

### 175 **2.3.3 *In situ* DOC bioavailability experiment**

176 The bioavailability experiment was conducted during fieldwork from August 17th to 31st, 2015 at  
 177 the glacier terminus. In brief, surface ice samples were collected in pre-combusted (550°C, 6 h)  
 178 aluminum basins and melted in the field. The melted samples were filtered through pre-combusted  
 179 glass fiber filters (GF/F 0.7  $\mu\text{m}$ ) into 12 pre-cleaned 125-mL polycarbonate bottles and wrapped with

180 three layers of aluminum foil to avoid solar irradiation. Two samples were refrigerated immediately  
181 after filtering to obtain initial DOC concentrations; the others were placed outside at the terminus of the  
182 glacier, and 2 samples were refrigerated every 3 days to obtain corresponding DOC values. The BDOC  
183 was calculated based on the discrepancies between the initial and treated samples.

## 184 **3 Results and discussion**

### 185 **3.1 DOC concentrations and bioavailability**

#### 186 **3.1.1 Snowpits**

187 The average DOC concentration in the snowpit samples was  $332 \pm 132 \mu\text{g L}^{-1}$  (Fig. 2), with values  
188 ranging from  $124 \mu\text{g L}^{-1}$  to  $581 \mu\text{g L}^{-1}$  (Fig. 3). The highest values occurred in the dirty layers (Fig. 3),  
189 similar to the pattern observed at the Greenland summit (Hagler et al., 2007) and in glaciers on the  
190 southern TP (Xu et al., 2013), indicating that DOC concentrations in the study area were probably  
191 influenced by desert sourced mineral dust deposition from adjacent arid regions and the frequent dust  
192 storms. Spatially, our results were higher than those of Xiaodongkemadi Glacier on Mountain Tanggula  
193 (TGL) in the central TP and the East Rongbu Glacier on Mount Everest (EV) on the southern TP (Fig.  
194 1) (Yan et al., 2015); however, they follow a similar pattern to that of the mercury distribution on the  
195 TP (Zhang et al., 2012a). In addition, the DOC concentrations on LHG Glacier were also higher than  
196 those of Mendenhall Glacier, Alaska (Stubbins et al., 2012) and the Greenland summit (Table 2)  
197 (Hagler et al., 2007).

#### 198 **3.1.2 Surface snow and ice**

199 The average DOC concentration in LHG glacier surface snow was significantly lower than that in  
200 surface ice because more impurities are present in the latter (Fig. 2). Like those of the snowpits, DOC  
201 concentrations in the glacier surface ice (Fig. 2) were higher than those on the southern TP  
202 (Nyainqentanglha Glacier) (Spencer et al., 2014) and subsurface ice (0.5 m beneath the glacier surface)  
203 in a European Alpine glacier (Singer et al., 2012) (Table 2) but comparable to that in the surface ice of  
204 the Antarctic Ice Sheet (Hood et al., 2015). However, the DOC concentrations in surface snow (Table 2)  
205 were higher than those in the Greenland Ice Sheet (Hagler et al., 2007), mainly due to the heavy dust  
206 load on LHG Glacier. No significant relationship was found between DOC concentration and elevation  
207 for either the surface snow or ice (Fig. S1), suggesting there is no link between altitude and DOC at this  
208 glacier. Similar weak correlation with altitude at LHG was also found with mercury (Huang et al.,  
209 2014). Therefore, the distributions of DOC concentrations in the glacier surface snow and ice were



210 influenced by other complex factors, such as different slopes (Hood and Scott, 2008) and cryoconite  
211 holes. Furthermore, DOC concentrations in snow and ice at this glacier were within the range of  
212 previously reported values for glacierized regions outside the TP.

### 213 **3.1.3 DOC bioavailability**

214 The *in situ* bioavailability experiment results showed that the amount of DOC being consumed  
215 decreased exponentially over time ( $R^2 = 0.98$ ) (Fig. 4), with approximately 26.7 % (from 417  $\mu\text{g L}^{-1}$  to  
216 306  $\mu\text{g L}^{-1}$ ) degraded within 15 days during the experiment (average temperature:  $3.8 \pm 3.7$  °C; range:  
217 -4.8 to 11.4 °C). The BDOC would have reached 46.3 % if the experiment duration was extended to 28  
218 days, according to the equation derived from the 15-day experiment (Fig. 4). Despite different  
219 incubation conditions, this result agrees well with the reports of BDOC from a glacier on the southern  
220 TP (28-day dark incubation at 20 °C, 46-69 % BDOC) (Spencer et al., 2014) and from European  
221 Alpine glaciers (50-day dark incubation at 4 °C,  $59 \pm 20$  % BDOC) (Singer et al., 2012). Therefore, the  
222 previous results obtained in the laboratory closely reflect *in situ* situation and can be used to estimate  
223 the bioavailability of glacier-derived DOC.

### 224 **3.2 Sources of snowpit DOC**

225 In this study, major ions were adopted as indicators to investigate the potential sources of snowpit  
226 DOC, because the sources of major ions in snowpit samples from Tibetan glaciers have previously  
227 been investigated in detail (Kang et al., 2002; Kang et al., 2008; Wu et al., 2011; Yan et al., 2015).  
228 Moreover, the DOC profiles in two snowpits varied with the dust content; specifically, DOC  
229 concentration of dust layers was much higher than that of clean layers. Furthermore, it was found that  
230 DOC and  $\text{Ca}^{2+}$  (a typical indicator of mineral dust (Yao, 2004)) were significantly correlated ( $R^2 = 0.84$ ,  
231 Fig. S2), suggesting that the major source of DOC was desert sourced mineral dust, similarly to the  
232 previous investigations of sources of snowpits at this glacier (Yan et al., 2015). Combined geochemical  
233 and backward trajectories analysis at LHG Glacier further supports the interpretation that dust particles  
234 on the glacier were mainly derived from the deserts to the west and north of the study area (Dong et al.,  
235 2014a; Dong et al., 2014b). Despite this potential source, local anthropogenic pollutants (biomass,  
236 fossil fuel combustion and other activities) (Yan et al., 2015) and biological activities on glacier surface  
237 (Anesio et al., 2009) may also contribute to the glacier DOC.

### 238 **3.3 Light absorption characteristics of DOC**

### 239 3.3.1 AAE

240 The Absorption Ångström Exponent (AAE) is generally used to characterize the spectral  
241 dependence of the light absorption of DOC, thereby providing important input data for radiative  
242 forcing calculations. The fitted  $AAE_{330-400}$  values ranged from 1.2 to 15.2 ( $5.0 \pm 5.9$ ) for snow samples  
243 and from 0.3 to 8.4 ( $3.4 \pm 2.7$ ) for ice samples (Fig. S4). The relatively low  $AAE_{330-400}$  values for ice  
244 indicated that the DOC had experienced strong photobleaching caused by long-term exposure to solar  
245 irradiation. Previous studies have found that the AAE values of brown carbon in aged aerosols (Zhao et  
246 al., 2015) and secondary organic aerosols (SOAs) (Lambe et al., 2013) were much lower than their  
247 respective primary values. Therefore, the wide divergence in AAE values might suggest different  
248 chemical compositions of DOC due to multiple factors, such as different sources and photobleaching  
249 processes. Regardless, the average AAE value of the snow samples was comparable to that of  
250 atmospheric aerosols in urban areas in South Asia (New Delhi, India) (Kirillova et al., 2014b) (Table 2).  
251 In general, the  $AAE_{330-400}$  values had a negative relationship with  $MAC_{365}$ , especially in the ice samples  
252 (Fig. S4), suggesting that the more strongly absorbing DOC might contribute to lower AAE values, as  
253 has been observed in previous aerosol studies (Chen and Bond, 2010; Bosch et al., 2014; Kirillova et  
254 al., 2014b).

### 255 3.3.2 $MAC_{365}$

256 The mass absorption cross section at 365 nm ( $MAC_{365}$ ) for DOC is another input parameter for the  
257 radiative forcing calculation. The light absorption ability at 365 nm was selected to avoid interferences  
258 of non-organic compounds (such as nitrate) and for consistency with previous investigations (Hecobian  
259 et al., 2010; Cheng et al., 2011). The  $MAC_{365}$  was  $1.4 \pm 0.4 \text{ m}^2 \text{ g}^{-1}$  in snow and  $1.3 \pm 0.7 \text{ m}^2 \text{ g}^{-1}$  in  
260 glacier ice (Fig. S4), both of which were higher than those of water soluble organic carbon in an  
261 outflow in northern China (Kirillova et al., 2014a) and on a receptor island in the Indian Ocean (Bosch  
262 et al., 2014). Meanwhile, the values were comparable to DOC concentrations in typical urban aerosols  
263 associated with biomass combustion in winter in Beijing, China (Cheng et al., 2011) and in New Delhi,  
264 India (Kirillova et al., 2014b) (Table 3). The MAC values for DOC from different sources vary widely.  
265 Typically, the  $MAC_{365}$  of DOC derived from biomass combustion can reach  $5 \text{ m}^2 \text{ g}^{-1}$  (Kirchstetter, 2004)  
266 (Table 3). Correspondingly, the values for SOAs can be as low as  $0.001\text{-}0.088 \text{ m}^2 \text{ g}^{-1}$  (Lambe et al.,  
267 2013). Due to the remote location of LHG Glacier, it was considered that the snowpit DOC should  
268 comprise SOAs with low  $MAC_{365}$  values; however, the high  $MAC_{365}$  value of the snowpit DOC

269 indicated that DOC may not be entirely derived from SOAs. Hence, it was proposed that mineral  
270 dust-sourced DOC caused the high  $MAC_{365}$  values in the snowpit samples. For instance, the light  
271 absorption characteristics of DOC from both snowpit and ice samples showed similar patterns to those  
272 of water soluble organic carbon in dust from the adjacent deserts, further indicating that LHG glacier  
273 DOC was transported via desert sourced mineral dust and shared similar light absorption characteristics  
274 (Fig. 5). Moreover, the difference in light absorption characteristics (especially for wavelengths larger  
275 than 400 nm) between snow/ice samples and aerosols in Beijing, China, also indicated their different  
276 sources (Fig. 5). Light absorbance was significantly correlated with DOC concentrations in both snow  
277 and ice samples (Fig. S3), indicating that DOC was one of the absorption factors. Nevertheless, the  
278  $MAC_{365}$  values of surface ice (0-3 cm) were lower than those of subsurface layers (3-5 cm), despite  
279 their higher DOC concentrations (Fig. 6), reflecting stronger DOC photobleaching in the surface ice  
280 due to the direct exposure to solar irradiation.

### 281 **3.3.3 Radiative forcing of DOC relative to BC**

282 Our results showed that the radiative forcing by DOC relative to that of BC ranged from 2.1 % to  
283 30.4 % ( $9.5 \pm 8.4$  %) for snowpit samples and from 0.01 % to 0.5 % ( $0.1 \pm 0.1\%$ ) for surface ice  
284 samples (Fig. S4). The high radiative forcing ratio of snowpit samples was caused by its higher  
285 DOC/BC (0.65) than that of surface ice (0.012) (Fig. S5), and the low ratio of DOC/BC in surface ice  
286 was caused by enrichment of BC in surface glacier ice during the intensive ablation period (Xu et al.,  
287 2009). Snowpit samples can be considered as broadly representative of fresh snow; thus, it is concluded  
288 that radiative forcing by DOC is a non-trivial contributor in addition to BC in reducing the albedo of a  
289 glacier when the glacier is covered by fresh snow. The snowpit samples can directly reflect the wet and  
290 dry deposition of atmospheric carbonaceous matter in glacierized regions, and the contribution of  
291 radiative forcing of snowpit DOC samples is comparable to that of water soluble organic carbon  
292 relative to BC in the atmosphere aerosols to some extent (Kirillova et al., 2014a), but lower than that of  
293 aerosols at the top of the atmosphere for the faster decrease of BC concentrations than brown carbon in  
294 the high-altitude atmosphere (Liu et al., 2014).

### 295 **3.4 DOC export during the melt season**

296 The two-year average discharge-weighted DOC concentration was  $238 \pm 96 \mu\text{g L}^{-1}$  during the  
297 melting period. Seasonally, high DOC concentrations appeared during the low discharge periods (May  
298 to July and September to October) (Fig. 7), suggesting that DOC concentrations were slightly enriched

299 to some extent. However, there were no clear diurnal variations in DOC concentrations with discharge,  
300 suggesting that the discharge from different parts of the glacier was well mixed at the glacier terminus  
301 (Fig. S6).

302 The seasonal variations in DOC flux were similar to those of the discharge (Fig. 7), indicating  
303 that discharge (rather than DOC concentrations) played a dominant role in the DOC mass flux. Hence,  
304 the majority of the glacier DOC export occurred during the summer melting season. Over the whole  
305 melting season, the annual flux of DOC from LHG Glacier was  $192 \text{ kg km}^{-2} \text{ yr}^{-1}$ , with peak DOC  
306 fluxes occurring from mid-late July to late August (70 % of the annual flux). When combined with the  
307 value of BDOC determined above, at least  $3211 \text{ kg C yr}^{-1}$  was ready to be decomposed and returned to  
308 the atmosphere as  $\text{CO}_2$  within one month of its release, producing positive feedback in the global  
309 warming process.

310 When considering the entire TP, it is obvious that proglacial streamwater DOC concentrations  
311 (Table S2) showed similar spatial variation to those of snowpit DOC (Li et al., 2016), with high and  
312 low value being observed on the northern and southern TP, respectively, reflecting strong association  
313 between proglacial streamwater DOC concentration and that of snowpit samples. Based on an average  
314 proglacial streamwater DOC concentration of  $193 \mu\text{g L}^{-1}$  (Table S2) and annual glacial meltwater  
315 runoff of  $66\text{-}68.2 \text{ km}^3$  in China (Xie et al., 2006), it was calculated that DOC flux in proglacial  
316 streamwater of the entire TP glacier was around  $12.7\text{-}13.2 \text{ Gg C}$  ( $\text{Gg} = 10^9 \text{ g}$ ). This estimate is higher  
317 than that of DOC deposition ( $5.6 \text{ Gg C}$ ) across the glacial region of the TP (Li et al., 2016), and agree  
318 well with the negative glaciers water balance of the TP. Therefore, the TP glaciers can be considered as  
319 a carbon source under present environmental conditions.

#### 320 **4 Conclusions and implications**

321 The concentrations and light absorption characteristics of DOC on a medium sized valley glacier  
322 on the northern TP were reported in this study. The mean DOC concentrations of snowpit samples,  
323 fresh snow, surface ice and proglacial streamwater were  $332 \pm 132 \mu\text{g L}^{-1}$ ,  $229 \pm 104 \mu\text{g L}^{-1}$ ,  $426 \pm 270$   
324  $\mu\text{g L}^{-1}$  and  $238 \pm 96 \mu\text{g L}^{-1}$ , respectively. These values were slightly higher than or comparable with  
325 those of other regions (e.g., European Alps and Alaska). DOC in snowpit samples was significantly  
326 correlated with  $\text{Ca}^{2+}$ , a typical cation in mineral dust, indicating that mineral dust transported from  
327 adjacent arid regions likely made important contributions to DOC of the studied glacierized regions. In  
328 addition, the light absorption profiles of the snowpit DOC was similar to that of dust from potential

329 source deserts. Based on the previously published radiative forcing data for black carbon in snowpit of  
330 LHG (Ming et al., 2013), it was estimated that the radiative forcing caused by snowpit DOC was 0.43  
331  $\text{W m}^{-2}$ , accounting for around 10 % of the radiative forcing caused by BC. Therefore, in addition to BC,  
332 DOC is also an important absorber of solar radiation in glacierized regions, especially when the glacier  
333 is covered by fresh snow. It has also been proven that water-insoluble organic carbon has stronger light  
334 absorption ability. Therefore, the total contribution of OC to light absorption in glacierized regions  
335 should be higher, which requires further study in the future.

336 Proglacial streamwater represented a well-mixed, integrated contribution from different parts of  
337 the glacier, so no clear diurnal variations in DOC concentrations were identified. Combined with  
338 discharge and the corresponding DOC concentration, it was calculated that approximate  $192.0 \text{ kg km}^{-2}$   
339  $\text{yr}^{-1}$  of DOC was released from LHG Glacier. It was also estimated that approximate 46.3 % of the  
340 DOC could be decomposed within 28 days; thus,  $3,211 \text{ kg C yr}^{-1}$  would return to the atmosphere as  
341  $\text{CO}_2$ , providing the potential for positive feedback in the warming process.

342

343 *Acknowledgements.* This study was supported by the National Nature Science Foundation of China (41225002,  
344 41271015, 41121001), State Key Laboratory of Cryospheric Science (SKLCS-ZZ-2015-10 and  
345 SKLCS-OP-2014-05) and the Academy of Finland (decision number 268170). The authors acknowledge the staff  
346 of the Qilian Shan Station of Glaciology and Ecological Environment, Chinese Academy of Science.

347

348

#### 349 **References**

- 350 Andreae, M. and Gelencsér, A.: Black carbon or brown carbon? The nature of light-absorbing carbonaceous  
351 aerosols, *Atmos. Chem. Phys.*, 6, 3131-3148, 2006.
- 352 Anesio, A. M., Hodson, A. J., Fritz, A., Psenner, R., and Sattler, B.: High microbial activity on glaciers: importance  
353 to the global carbon cycle, *Global Change Biol.*, 15, 955-960, 2009.
- 354 Anesio, A. M. and Laybourn-Parry, J.: Glaciers and Ice Sheets as a biome, *Trends Ecol. Evol.*, 27, 219-225, 2012.
- 355 Antony, R., Grannas, A. M., Willoughby, A. S., Sleighter, R. L., Thamban, M., and Hatcher, P. G.: Origin and  
356 sources of dissolved organic matter in snow on the East Antarctic Ice Sheet, *Environ. Sci. Technol.*, 48,  
357 6151-6159, 2014.
- 358 Antony, R., Mahalinganathan, K., Thamban, M., and Nair, S.: Organic Carbon in Antarctic Snow: Spatial Trends  
359 and Possible Sources, *Environ. Sci. Technol.*, 45, 9944-9950, 2011.
- 360 Bhatia, M. P., Das, S. B., Longnecker, K., Charette, M. A., and Kujawinski, E. B.: Molecular characterization of  
361 dissolved organic matter associated with the Greenland Ice Sheet, *Geochim. Cosmochim. Acta.*, 74, 3768-3784,  
362 2010.

363 Bolch, T., Kulkarni, A., Kaab, A., Huggel, C., Paul, F., Cogley, J. G., Frey, H., Kargel, J. S., Fujita, K., Scheel, M.,  
364 Bajracharya, S., and Stoffel, M.: The state and fate of Himalayan glaciers, *Science*, 336, 310-314, 2012.

365 Bond, T. C., and Bergstrom, R. W.: Light Absorption by Carbonaceous Particles: An Investigative Review, *Aerosol*  
366 *Sci. Technol.*, 40, 27-67, 10.1080/02786820500421521, 2006.

367 Bosch, C., Andersson, A., Kirillova, E. N., Budhavant, K., Tiwari, S., Praveen, P., Russell, L. M., Beres, N. D.,  
368 Ramanathan, V., and Gustafsson, Ö.: Source-diagnostic dual-isotope composition and optical properties of  
369 water-soluble organic carbon and elemental carbon in the South Asian outflow intercepted over the Indian  
370 Ocean, *J. Geophys. Res. Atmos.*, 119, 743-711,759, 2014.

371 Chen, Y. and Bond, T. C.: Light absorption by organic carbon from wood combustion, *Atmos. Chem. Phys.*, 10,  
372 1773-1787, 2010.

373 Cheng, Y., He, K. B., Zheng, M., Duan, F. K., Du, Z. Y., Ma, Y. L., Tan, J. H., Yang, F. M., Liu, J. M., Zhang, X. L.,  
374 Weber, R. J., Bergin, M. H., and Russell, A. G.: Mass absorption efficiency of elemental carbon and  
375 water-soluble organic carbon in Beijing, China, *Atmos. Chem. Phys.*, 11, 11497-11510, 2011.

376 Dong, Z., Qin, D., Chen, J., Qin, X., Ren, J., Cui, X., Du, Z., and Kang, S.: Physicochemical impacts of dust  
377 particles on alpine glacier meltwater at the Laohugou Glacier basin in western Qilian Mountains, China, *Sci.*  
378 *Total Environ.*, 493, 930-942, 2014a.

379 Dong, Z., Qin, D., Kang, S., Ren, J., Chen, J., Cui, X., Du, Z., and Qin, X.: Physicochemical characteristics and  
380 sources of atmospheric dust deposition in snow packs on the glaciers of western Qilian Mountains, China, *Tellus*  
381 *B*, 66, 2014b.

382 Du, W., Qin, X., Liu, Y. S., and Wang, X. F.: Variation of Laohugou Glacier No. 12 in Qilian Mountains, *Journal of*  
383 *Glaciology and Geocryology*, 30, 373-379, 2008 (in Chinese with English abstract).

384 Hagler, G. S. W., Bergin, M. H., Smith, E. A., Dibb, J. E., Anderson, C., and Steig, E. J.: Particulate and  
385 water-soluble carbon measured in recent snow at Summit, Greenland, *Geophys. Res. Lett.*, 34, L16505,  
386 doi:10.1029/2007GL030110, 2007.

387 Hattori, Y., Suzuki, K., Honda, M., and Shimizu, H.: Re-Os isotope systematics of the Taklimakan Desert sands,  
388 moraines and river sediments around the Taklimakan Desert, and of Tibetan soils, *Geochim. Cosmochim. Acta.*,  
389 67, 1203-1213, 2003.

390 Hecobian, A., Zhang, X., Zheng, M., Frank, N., Edgerton, E. S., and Weber, R. J.: Water-Soluble Organic Aerosol  
391 material and the light-absorption characteristics of aqueous extracts measured over the Southeastern United  
392 States, *Atmos. Chem. Phys.*, 10, 5965-5977, 2010.

393 Hood, E., Battin, T. J., Fellman, J., O'Neel, S., and Spencer, R. G. M.: Storage and release of organic carbon from  
394 glaciers and ice sheets, *Nat. Geosci.*, 8, 91-96, 2015.

395 Hood, E., Fellman, J., Spencer, R. G., Hernes, P. J., Edwards, R., D'Amore, D., and Scott, D.: Glaciers as a source  
396 of ancient and labile organic matter to the marine environment, *Nature*, 462, 1044-1047, 2009.

397 Hood, E. and Scott, D.: Riverine organic matter and nutrients in southeast Alaska affected by glacial coverage, *Nat.*  
398 *Geosci.*, 1, 583-587, 2008.

399 Huang, J., Kang, S., Guo, J., Sillanpää, M., Zhang, Q., Qin, X., Du, W., and Tripathee, L.: Mercury distribution  
400 and variation on a high-elevation mountain glacier on the northern boundary of the Tibetan Plateau, *Atmos.*  
401 *Environ.*, 96, 27-36, 2014.

402 Jacob, T., Wahr, J., Pfeffer, W. T., and Swenson, S.: Recent contributions of glaciers and ice caps to sea level rise,  
403 *Nature*, 482, 514-518, 2012.

404 Kang, S., Huang, J., and Xu, Y.: Changes in ionic concentrations and  $\delta^{18}\text{O}$  in the snowpack of Zhadang glacier,  
405 Nyainqentanglha mountain, southern Tibetan Plateau, *Ann. Glaciol.*, 49, 127-134, 2008.

406 Kang, S., Mayewski, P. A., Qin, D., Yan, Y., Hou, S., Zhang, D., Ren, J., and Kruetz, K.: Glaciochemical records

407 from a Mt. Everest ice core: relationship to atmospheric circulation over Asia, *Atmos. Environ.*, 36, 3351-3361,  
408 2002.

409 Kang, S., Wang, F., Morgenstern, U., Zhang, Y., Grigholm, B., Kaspari, S., Schwikowski, M., Ren, J., Yao, T., Qin,  
410 D., and Mayewski, P. A.: Dramatic loss of glacier accumulation area on the Tibetan Plateau revealed by ice core  
411 tritium and mercury records, *The Cryosphere*, 9, 1213-1222, 2015.

412 Kaspari, S., Painter, T. H., Gysel, M., Skiles, S. M., and Schwikowski, M.: Seasonal and elevational variations of  
413 black carbon and dust in snow and ice in the Solu-Khumbu, Nepal and estimated radiative forcings, *Atmos.*  
414 *Chem. Phys.*, 14, 8089-8103, 2014.

415 Kehrwald, N. M., Thompson, L. G., Tandong, Y., Mosley-Thompson, E., Schotterer, U., Alfimov, V., Beer, J.,  
416 Eikenberg, J., and Davis, M. E.: Mass loss on Himalayan glacier endangers water resources, *Geophys. Res. Lett.*,  
417 35, L22503, doi: 10.1029/2008GL035556, 2008.

418 Kirchstetter, T. W.: Evidence that the spectral dependence of light absorption by aerosols is affected by organic  
419 carbon, *J. Geophys. Res.*, 109, D21208, doi: 10.1029/2004JD004999, 2004.

420 Kirillova, E. N., Andersson, A., Han, J., Lee, M., and Gustafsson, Ö.: Sources and light absorption of water-soluble  
421 organic carbon aerosols in the outflow from northern China, *Atmos. Chem. Phys.*, 14, 1413-1422, 2014a.

422 Kirillova, E. N., Andersson, A., Tiwari, S., Srivastava, A. K., Bisht, D. S., and Gustafsson, Ö.: Water-soluble  
423 organic carbon aerosols during a full New Delhi winter: Isotope-based source apportionment and optical  
424 properties, *J. Geophys. Res. Atmos.*, 119, 3476-3485, 2014b.

425 Lambe, A. T., Cappa, C. D., Massoli, P., Onasch, T. B., Forestieri, S. D., Martin, A. T., Cummings, M. J., Croasdale,  
426 D. R., Brune, W. H., and Worsnop, D. R.: Relationship between oxidation level and optical properties of  
427 secondary organic aerosol, *Environ. Sci. Technol.*, 47, 6349-6357, 2013.

428 Lau, W. K. M., Kim, M.-K., Kim, K.-M., and Lee, W.-S.: Enhanced surface warming and accelerated snow melt in  
429 the Himalayas and Tibetan Plateau induced by absorbing aerosols, *Environ. Res. Lett.*, 5, 025204,  
430 doi:10.1088/1748-9326/5/2/025204, 2010.

431 Lawson, E. C., Wadham, J. L., Tranter, M., Stibal, M., Lis, G. P., Butler, C. E. H., Laybourn-Parry, J., Nienow, P.,  
432 Chandler, D., and Dewsbury, P.: Greenland Ice Sheet exports labile organic carbon to the Arctic oceans,  
433 *Biogeosci.*, 11, 4015-4028, 2014.

434 Legrand, M., Preunkert, S., Jourdain, B., Guilhermet, J., Fain, X., Alekhina, I., and Petit, J. R.: Water-soluble  
435 organic carbon in snow and ice deposited at Alpine, Greenland, and Antarctic sites: a critical review of available  
436 data and their atmospheric relevance, *Clim. Past Discuss.*, 9, 2357-2399, 2013.

437 Levinson, R., Akbari, H., and Berdahl, P.: Measuring solar reflectance—Part I: Defining a metric that accurately  
438 predicts solar heat gain, *Sol. Energy*, 84, 1717-1744, 2010.

439 Li, C., Chen, P., Kang, S., Yan, F., Li, X., Qu, B., and Sillanpää, M.: Carbonaceous matter deposition in the high  
440 glacial regions of the Tibetan Plateau, *Atmos. Environ.*, 141, 203-208, 2016.

441 Li, C., Kang, S., Zhang, Q., and Kaspari, S.: Major ionic composition of precipitation in the Nam Co region,  
442 Central Tibetan Plateau, *Atmos. Res.*, 85, 351-360, 2007.

443 Li, J., Qin, X., Sun, W., zhang, M., and Yang, J.: Analysis on Micrometeorological Characteristic in the Surface  
444 Layer of Laohugou Glacier No.12 Qilian Mountains, *Plateau Meteorology*, 31, 370-379, 2012.

445 Li, Z., Li, H., Dong, Z., and Zhang, M.: Chemical characteristics and environmental significance of fresh snow  
446 deposition on Urumqi Glacier No. 1 of Tianshan Mountains, China, *Chinese Geographical Science*, 20, 389-397,  
447 2010.

448 Liu, J., Scheuer, E., Dibb, J., Ziemba, L. D., Thornhill, K., Anderson, B. E., Wisthaler, A., Mikoviny, T., Devi, J. J.,  
449 and Bergin, M.: Brown carbon in the continental troposphere, *Geophys. Res. Lett.*, 41, 2191-2195, 2014.

450 May, B., Wagenbach, D., Hoffmann, H., Legrand, M., Preunkert, S., and Steier, P.: Constraints on the major

451 sources of dissolved organic carbon in Alpine ice cores from radiocarbon analysis over the bomb - peak period,  
452 *J. Geophys. Res. Atmos.*, 118, 3319-3327, 2013.

453 Ming, J., Xiao, C., Du, Z., and Yang, X.: An overview of black carbon deposition in High Asia glaciers and its  
454 impacts on radiation balance, *Adv. Water Resour.*, 55, 80-87, 2013.

455 Nair, V. S., Babu, S. S., Moorthy, K. K., Sharma, A. K., Marinoni, A., and Ajai: Black carbon aerosols over the  
456 Himalayas: direct and surface albedo forcing, *Tellus B*, 65, <http://dx.doi.org/10.3402/tellusb.v65i0.19738>, 2013.

457 Neckel, N., Kropáček, J., Bolch, T., and Hochschild, V.: Glacier mass changes on the Tibetan Plateau 2003–2009  
458 derived from ICESat laser altimetry measurements, *Environmental Research Letters*, 9, 014009, doi:10.1088/  
459 1748-9326/9/1/014009, 2014.

460 Qu, B., Ming, J., Kang, S. C., Zhang, G. S., Li, Y. W., Li, C. D., Zhao, S. Y., Ji, Z. M., and Cao, J. J.: The  
461 decreasing albedo of the Zhadang glacier on western Nyainqentanglha and the role of light-absorbing impurities,  
462 *Atmos. Chem. Phys.*, 14, 11117-11128, 2014.

463 Singer, G. A., Fasching, C., Wilhelm, L., Niggemann, J., Steier, P., Dittmar, T., and Battin, T. J.: Biogeochemically  
464 diverse organic matter in Alpine glaciers and its downstream fate, *Nat. Geosci.*, 5, 710-714, 2012.

465 Spencer, R. G. M., Guo, W., Raymond, P. A., Dittmar, T., Hood, E., Fellman, J., and Stubbins, A.: Source and  
466 biolability of ancient dissolved organic matter in glacier and lake ecosystems on the Tibetan Plateau, *Geochim.*  
467 *Cosmochim. Acta*, 142, 64-74, 2014.

468 Spencer, R. G. M., Stubbins, A., Hernes, P. J., Baker, A., Mopper, K., Aufdenkampe, A. K., Dyda, R. Y., Mwamba,  
469 V. L., Mangangu, A. M., and Wabakanghanzi, J. N.: Photochemical degradation of dissolved organic matter and  
470 dissolved lignin phenols from the Congo River, *J. Geophys. Res. Biogeosci.*, 114, 2009.

471 Stubbins, A., Hood, E., Raymond, P. A., Aiken, G. R., Sleighter, R. L., Hernes, P. J., Butman, D., Hatcher, P. G.,  
472 Striegl, R. G., Schuster, P., Abdulla, H. A. N., Vermilyea, A. W., Scott, D. T., and Spencer, R. G. M.:  
473 Anthropogenic aerosols as a source of ancient dissolved organic matter in glaciers, *Nat. Geosci.*, 5, 198-201,  
474 2012.

475 Wu, X., LI, Q., Wang, L., Pu, J., He, J., and Zhang, C.: Regional characteristics of ion concentration in glacial  
476 snowpits over the Tibetan Plateau and source analysis, *Environment Science*, 32, 971-975, 2011 (in Chinese  
477 with English abstract).

478 Xie, Z., Wang, X., Kang, E., Feng, Q., Li, Q., and Cheng, L.: Glacial runoff in China: an evaluation and prediction  
479 for the future 50 years, *Journal of Glaciology and Geocryology*, 28, 457-466, 2006.

480 Xu, B., Cao, J., Hansen, J., Yao, T., Joswia, D. R., Wang, N., Wu, G., Wang, M., Zhao, H., and Yang, W.: Black  
481 soot and the survival of Tibetan glaciers, *PNAS*, 106, 22114-22118, 2009.

482 Xu, J., Zhang, Q., Li, X., Ge, X., Xiao, C., Ren, J., and Qin, D.: Dissolved organic matter and inorganic ions in a  
483 central Himalayan glacier--insights into chemical composition and atmospheric sources, *Environ Sci Technol*,  
484 47, 6181-6188, 2013.

485 Yan, F., Kang, S., Chen, P., Li, Y., Hu, Z., and Li, C.: Concentration and source of dissolved organic carbon in  
486 snowpits of the Tibetan Plateau, *Environmental Science*, 8, 2827-2832, 2015.

487 Yao, T.: Relationship between calcium and atmospheric dust recorded in Guliya ice core, *Chin. Sci. Bull.*, 49,  
488 706-710, 2004.

489 Yao, T., Thompson, L., Yang, W., Yu, W., Gao, Y., Guo, X., Yang, X., Duan, K., Zhao, H., Xu, B., Pu, J., Lu, A.,  
490 Xiang, Y., Kattel, D. B., and Joswiak, D.: Different glacier status with atmospheric circulations in Tibetan  
491 Plateau and surroundings, *Nat. Clim. Change*, doi: 10.1038/nclimate1580, 2012.

492 Zhang, Q., Huang, J., Wang, F., Mark, L., Xu, J., Armstrong, D., Li, C., Zhang, Y., and Kang, S.: Mercury  
493 distribution and deposition in glacier snow over western China, *Environ. Sci. Technol.*, 46, 5404-5413, 2012a.

494 Zhang, Y., Liu, S., Shangguan, D., Li, J., and Zhao, J.: Thinning and shrinkage of Laohugou No. 12 glacier in the



495 Western Qilian Mountains, China, from 1957 to 2007, *Journal of Mountain Science*, 9, 343-350, 2012b.  
496 Zhao, R., Lee, A. K. Y., Huang, L., Li, X., Yang, F., and Abbatt, J. P. D.: Photochemical processing of aqueous  
497 atmospheric brown carbon, *Atmos. Chem. Phys. Discuss.*, 15, 2957-2996, 2015.  
498

**Table 1.** Sampling information for snow, ice and proglacial streamwater in this study.

Sample type	Sampling time	Resolution <sup>*</sup>	Sampling site	Number (n)	Index
Snowpit	30th July, 2014	5 cm	4989 m	15	DOC, absorbance, ions
Snowpit	25th August, 2015	5 cm	5050 m	23	DOC, absorbance, ions
Surface fresh snow	4th August, 2014	100 m	4450-4900 m	18	DOC
Surface ice	6th August, 2014	100 m	4350-4900 m	20	DOC
Surface snow	16th July, 2015	50 m	4350-4850 m	11	DOC
Surface ice	15th August, 2015	50 m	4350-4850 m	11	DOC
Surface ice	25th August, 2015	50 m	4350-4600 m	6	DOC, absorbance
Subsurface ice	25th August, 2015	50 m	4350-4600 m	5	DOC, absorbance
Proglacial streamwater	29th-30th July, 2014	2h (day),4h (night)	4210 m	17	DOC
Proglacial streamwater	20th May-9th October, 2015	Every day	4210 m	184	DOC

500 <sup>\*</sup> Vertical resolution (snowpit) or horizontal distance (surface snow and ice).

501

502

503  
504

**Table 2.** Comparison of DOC concentrations in snow, ice and proglacial streamwater from the glacier in this study and glaciers in other regions.

Sites	DOC concentration ( $\mu\text{g L}^{-1}$ )	Sample types	References
Laohugou Glacier (LHG)	$332 \pm 132$	Snowpit	This study
Tanggula Glacier (TGL)	$217 \pm 143$	Snowpit	Yan et al. (2015)
Mount Everest (EV)	$153 \pm 561$	Snowpit	
Mendenhall Glacier, Alaska	190	snowpit	Stubbins et al. (2012)
Greenland Ice Sheet	401 - 57	Snowpit	Hagler et al. (2007)
Laohugou Glacier (LHG)	$229 \pm 104$	Surface snow	This study
Greenland Ice Sheet	111	Surface snow	Hagler et al. (2007)
Juneau Icefield, Southeast Alaska	100 - 300	Fresh snow/snowpits	Fellman et al. (2015)
Laohugou Glacier (LHG)	$426 \pm 270$	Surface ice	This study
Mount Nyainqentanglha Glacier	212	Glacier ice	Spencer et al. (2014)
Antarctic Ice Sheet	$460 \pm 120$	Surface ice	Hood et al. (2015)
Alpine glacier	$138 \pm 96$	Subsurface ice	Singer et al. (2012)
Laohugou Glacier (LHG)	$238 \pm 96$	Proglacial streamwater	This study
Mount Nyainqentanglha Glacier	262	Proglacial streamwater	Spencer et al. (2014)
Mendenhall Glacier, Alaska	$380 \pm 20$	Proglacial streamwater	Stubbins et al. (2012)

505  
506

507 **Table 3.** Mass absorption cross section (MAC) and Absorption Ångström Exponent (AAE<sub>330-400</sub>) of ice and snow  
 508 from LHG Glacier and aerosols from other regions.

Site/Source	MAC (m <sup>2</sup> g <sup>-1</sup> )	AAE <sub>330-400</sub>	λ (MAC)	References
LHG Glacier	1.4 ± 0.4 (snow)	5.0 ± 5.9 (snow)	365	This study
	1.3 ± 0.7 (ice)	3.4 ± 2.7 (ice)		
Biomass smoke	5.0	4.8	350	Kirchstetter et al. (2004)
Secondary organic aerosols	0.001 - 0.088	5.2 - 8.8	405	Lambe et al. (2013)
Wood smoke	0.13 - 1.1	8.6 - 17.8	400	Chen and Bond (2010)
HULIS, Arctic snow	2.6 ± 1.1	6.1 <sup>*</sup>	250	Voisin et al. (2012)
Beijing, China (winter)	1.79 ± 0.24	7.5	365	Cheng et al. (2011)
Beijing, China (summer)	0.71 ± 0.20	7.1	365	Cheng et al. (2011)

509 <sup>\*</sup> The wavelength range for AAE in this study is 300 - 550 nm.

510

511

512 Figure 1. Location map of LHG Glacier No. 12.  
513 Figure 2. Average DOC concentrations of ice, snow and proglacial streamwater for LHG Glacier.  
514 Figure 3. Variation in DOC concentrations in profiles of studied snowpits. The gray rectangles are dirty layers.  
515 Figure 4. Exponential decreases in DOC concentrations during the biodegradation experiment. Note: The blue point  
516 is calculated using equations derived from the experimental data (black point).  
517 Figure 5. Absorption spectra for DOC in snow and ice of LHG Glacier and the dust from surrounding areas.  
518 Figure 6. Comparison of DOC concentrations (A) and  $MAC_{365}$  (B) between surface and subsurface ice.  
519 Figure 7. The discharge, DOC concentrations and fluxes exported from LHG Glacier. Note: The concentrations  
520 with error bars are used for days with more than one sample.  
521  
522

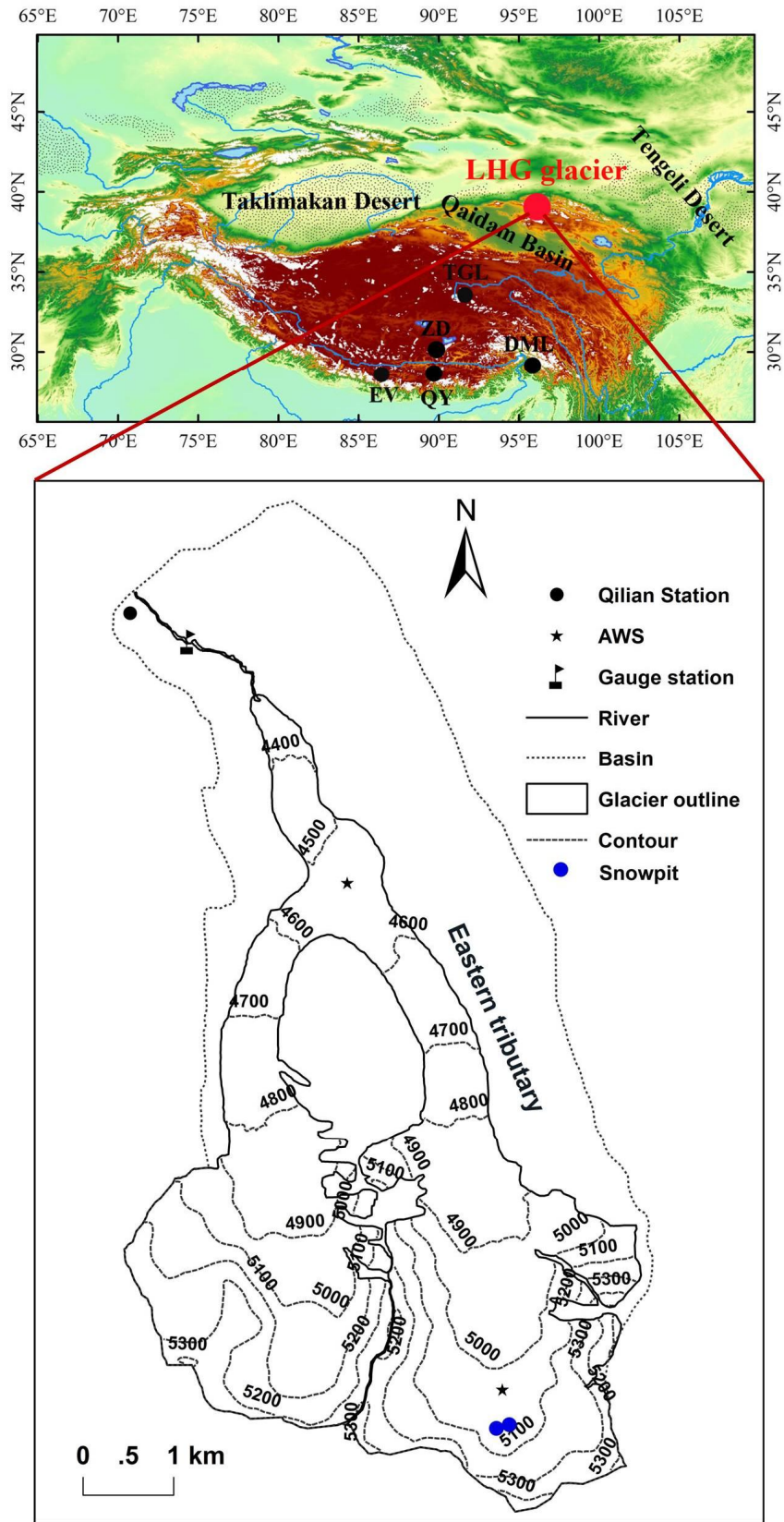
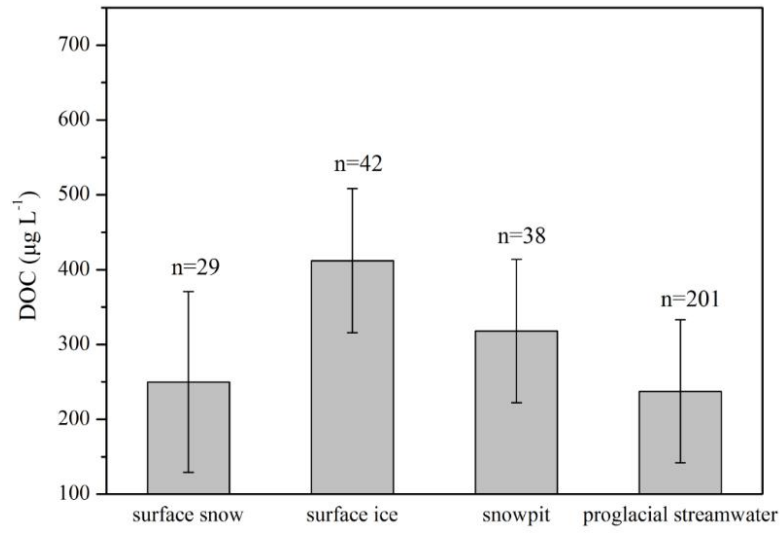


Figure 1. Location map of Laohugou glacier No. 12.

523

524

525



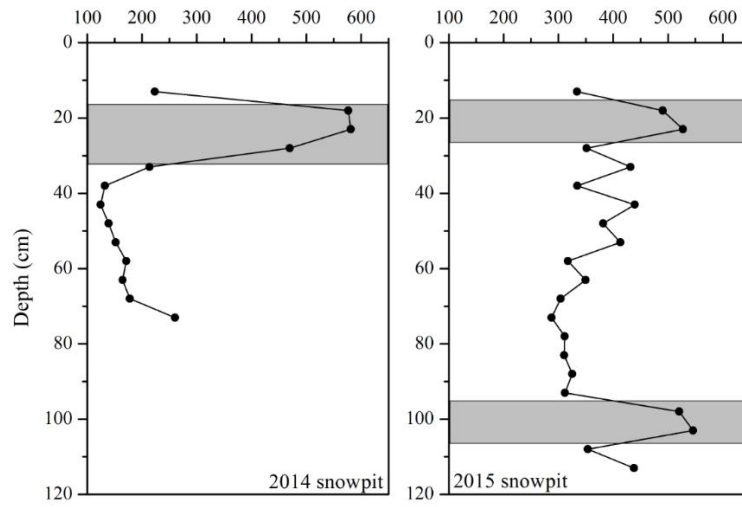
526

527

528

**Figure 2.** Average DOC concentrations of ice, snow and proglacial streamwater for LHG Glacier.

529



530

531 **Figure 3.** Variation in DOC concentrations in profiles of studied snowpits. The gray rectangles are dirty  
532 layers.

533

534

535

536

537

538

539

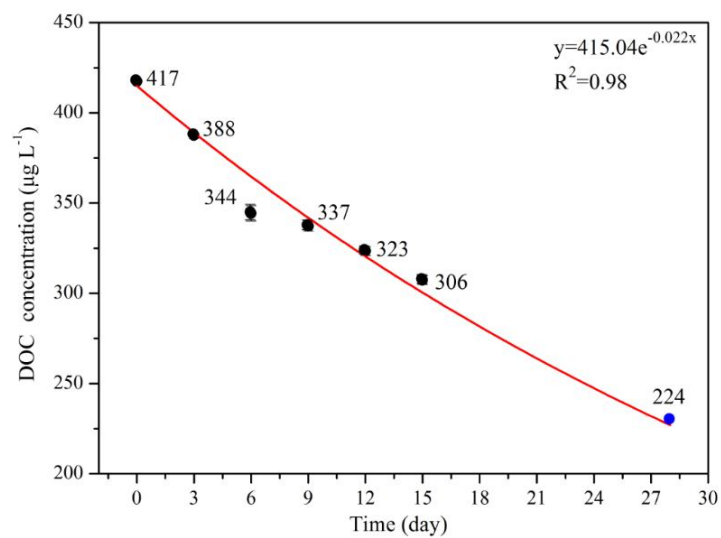
540

541



542

543



544

545

**Figure 4.** Exponential decreases in DOC concentrations during the biodegradation experiment. Note: The blue

546

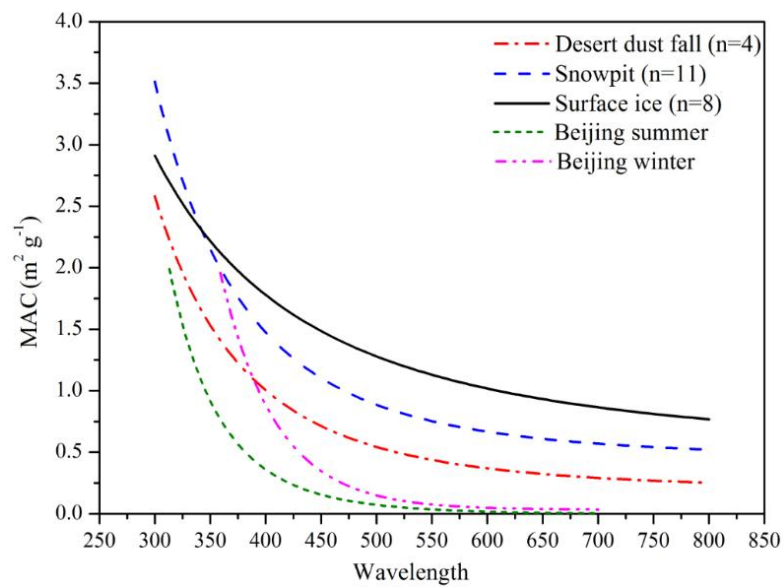
point is calculated using equations derived from the experimental data (black point). Mean values  $\pm$  standard

547

deviations of duplicate treated samples are presented.

548

549



550

551

552

553

554

**Figure 5.** Absorption spectra for DOC in snow and ice of LHG Glacier and the dust from surrounding areas.

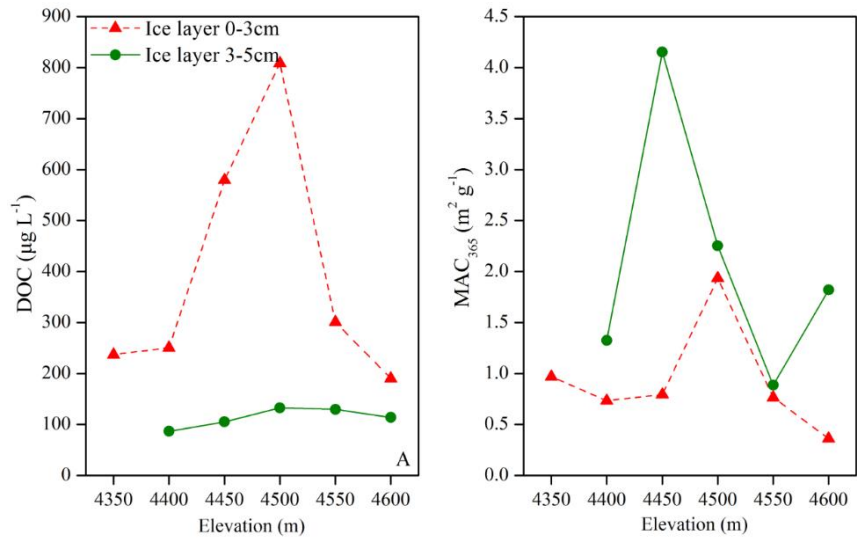
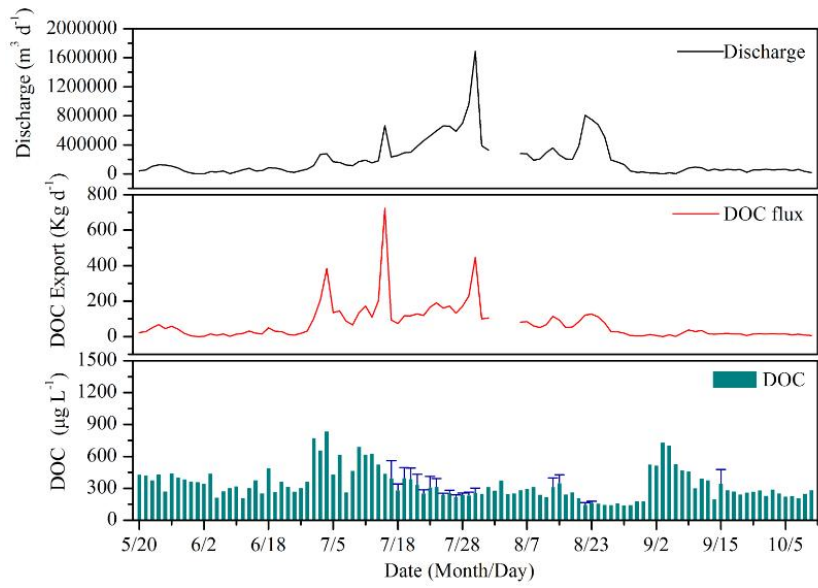


**Figure 6.** Comparison of DOC concentrations (A) and  $\text{MAC}_{365}$  (B) between surface and subsurface ice.

555  
 556  
 557  
 558



559

560

561

**Figure 7.** The discharge, DOC concentrations and fluxes exported from LHG Glacier. Note: The concentrations with error bars are used for days with more than one sample.

562

563